

# CATHODE GEOMETRY AND FLOW DYNAMICS IMPACT ON VERTICAL ELECTROPOLISHING OF SUPERCONDUCTING NIOBIUM CAVITIES

Leonel Marques Antunes Ferreira<sup>#</sup>, CERN, Geneva, Switzerland

## Abstract

CERN has now a fully operating vertical electropolishing installation, which has been used for the processing of 704 MHz high-beta five-cell Superconducting Proton Linac (SPL) niobium cavities. This installation relies only on the electrolyte circulation (HF/H<sub>2</sub>SO<sub>4</sub>) for power dissipation, evacuation of gases and homogeneous finishing; thus, parameters like cathode geometry, electrolyte flow and temperature become even more crucial when compared with horizontal electropolishing installations. Based on computational simulations performed with Comsol Multiphysics® and on a methodology developed at CERN, it is possible to assess the impact of the different cathode geometries as well as of the flow on the etching rate distribution. The data obtained with two different cathode geometries are presented: electrolyte velocity distribution, etching rate distribution, average current density and minimum working potential. One geometry was defined through a purely electrochemical approach while the second was defined to minimise the difference between the maximum and the minimum electrolyte speed inside the cavity; in both cases, the influence of the electrolyte flow was taken into account.

## INTRODUCTION

The most interesting electrochemical characteristic of the Siemens bath formulation [1] is the absence of a transpassivation behaviour in the anodic branch of its polarisation curve, see Figure 1. The main outcome is that for a very large range of anodic overpotential, the anodic dissolution yield is 100%; in other words there are no secondary reactions taking place other than the dissolution of niobium. Unlike many other electropolishing (EP) bath formulations, there is no formation of molecular oxygen at the surface and thus, pinholes and related surface defects are less prone to appear and surely not related to anodic oxygen evolution.

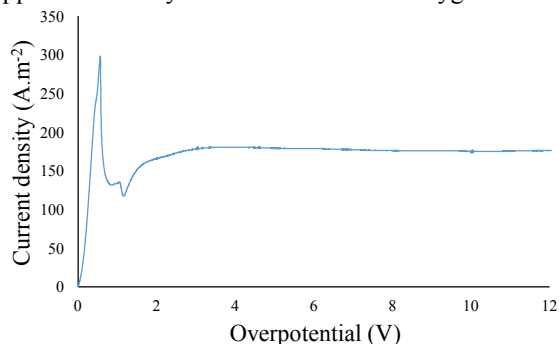


Figure 1: Anodic polarisation curve measured at 25 °C.

<sup>#</sup>leonel.ferreira@cern.ch

The described bath property plus the possibility to fully simulate the electrochemical polishing has guided CERN to exploit the processing of niobium SRF cavities in a vertical installation [2]. The objective, is to achieve the same performances as of horizontal installations, but with the advantage of a simplified set-up. CERN vertical EP installation relies only on the electrolyte circulation for power dissipation, gases evacuation and homogeneous finishing; thus, making it very simple to operate, but on the other hand, more difficult to tune up. With this constraint, the main optimisation parameters are the cathode geometry and the bath flow. The data and results achieved so far on SPL 704 MHz 5 cell cavities are presented hereafter.

## CATHODE GEOMETRY

Two cathode geometries were used so far to process SPL 5 cell cavities. The first geometry was designed taking into account only electrochemical parameters and it'll be referred as the electrochemical cathode (EC); a detailed explanation can be found elsewhere [3]. The surface finishing achieved with this cathode was bright and smooth, but macrostructures were apparent and could be related both to the bath flow and gas bubbles in the circulating bath; see Figure 2. From this experimental result, a reassessment of the cathode geometry was undertaken; laboratory trials and simulation work were developed to understand better the bath velocity distribution inside the cavity as well as to its impact on the polishing rate; the latter was already presented for the EC geometry [4].



Figure 2: Macrostructures on cavity SPL #1.

The SPL cavity geometry cannot be modified and it implies already significant bath velocity differences between the equator (wider section) and the iris (narrower section); the cathode geometry cannot improve the bath velocity distribution, but its impact can be minimised. Taking this principle into account, a second cathode geometry was defined: cylindrical hollow shape, the hollow cathode (HC); this approach is still able to provide sufficient cross section for the total applied current and minimises its impact on the bath velocity distribution

across the SPL cavity. A feature was also added to the HC, a PFE 70  $\mu\text{m}$  mesh membrane; it's intended to minimise the contact of hydrogen gas bubbles, which are produced at the cathode, with the cavity surface. Hydrogen bubbles are commonly [5, 6] considered as responsible for the formation of pinholes and other macrostructures on the cavity surface. Figures 3 and 4 presents the geometry of the two cathodes.

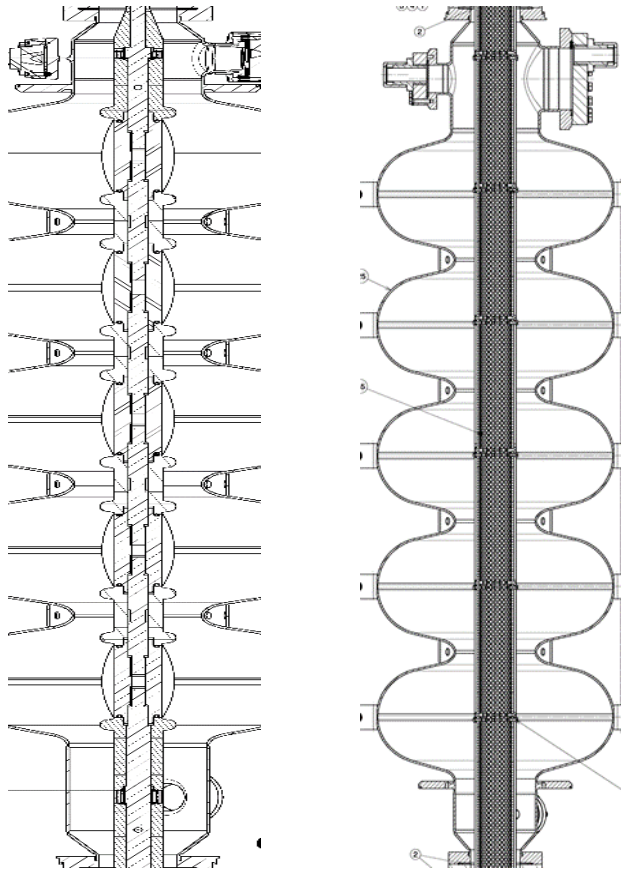


Figure 3: EC (left) and HC (right) geometries, both inserted in a SPL five cell cavity.

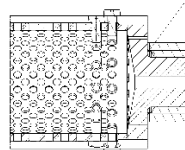
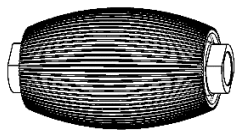


Figure 4: EC (left) and HC (right) cathode active surfaces.

### BATH FLOW

The HC geometry was defined and validated for production by comparing several fluid dynamic simulations done on the new HC and on the EC geometry. The data presented hereafter are a summary of the most representative ones.

#### Bath Speed Distribution

Figure 5 gives a general view of the bath speed distribution for both geometries at 20 and 10 litres per

minute (lpm). 20 lpm was the average flow used to process SPL #1 cavity, while 10 lpm arrives from a bath temperature constraint that is explained hereafter. The four different cases are an axisymmetric representation of the SPL fourth cell and the bath speed distribution is described by a rainbow of colours going from dark red (higher speed) to dark blue (lower speed); the same colour represents the same bath speed in all four different cases.

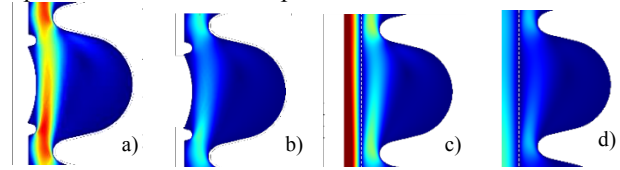


Figure 5: a) EC at 20 lpm; b) EC at 10 lpm; c) HC at 20 lpm; HC at 10 lpm.

For the same flow values, the purely electrochemical optimised proposal (see Figures 5a and 5b) shows sharper bath speed behaviour near the iris, if compared with the hollow cathode solution (see Figures 5c and 5d). It's also evident that at lower flow rates, and independently of the cathode geometry, the bath speed distribution becomes more uniform. Here, the main constraint for further reducing the bath flow is that the bath temperature depends on its flow rate; the latter cannot be fixed independently of the electrolyte temperature constraints, namely a maximum of 15  $^{\circ}\text{C}$  and with a differential between the inlet and the out let below 5  $^{\circ}\text{C}$ . Practical evidence showed that 10 lpm was, in average, the minimum flow allowed to respect the temperature constraints as defined above.

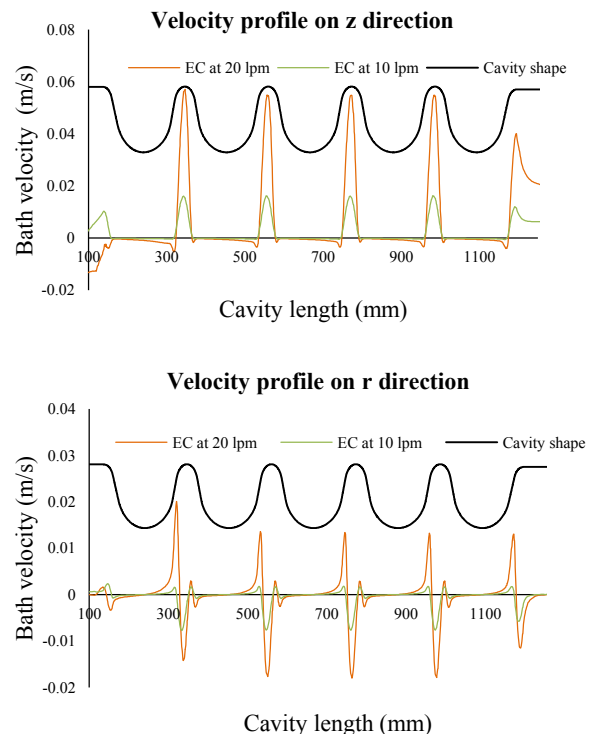


Figure 6: Bath velocity components profile for the EC geometry at 10 and 20 lpm.

Figures 6, 7 and 8 are representations of the bath velocity profile in the axial (z) and radial (r) directions, taken at 5 mm away from the cavity wall, through the cavity length. For all figures, it's an horizontal representation of a vertical setup, where the left represents the bath inlet (bottom) and the right the bath outlet (top); negative values represent downwards bath movements for z representations or bath movement towards the cathode for r representations; the black line is an axisymmetric representation of the SPL cavity wall where the symmetry axis lies above it; its shape might change slightly from figure to figure due to different axis bounds.

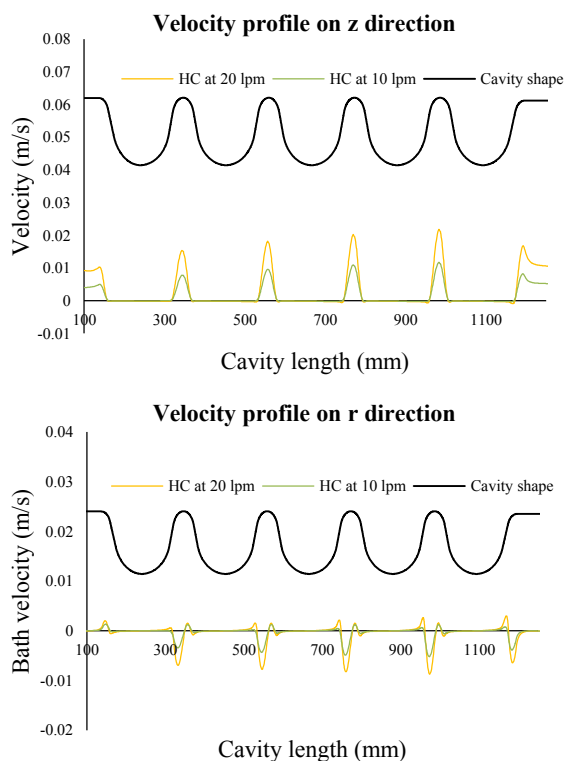


Figure 7: Bath velocity components profile for the HC geometry at 10 and 20 lpm.

As already mentioned, lower flow rates allow for a more homogeneous bath velocity distribution; this is even more evident for the EC (Fig. 6) which was not optimised for fluid dynamics and where the z velocity peak decreases roughly to 1/3 of its value at 20 lpm when the flow is only reduced to half (10 lpm). Fluid dynamic features called vortices, which are characterised by a sharp change in the velocity direction (+/-) are clearly identified just before and after the iris. The vortices are still more evident on the EC cathode at 20 lpm if compared with the 10 lpm; namely, and following the bath flow from left to right, for the ones just before irises. This feature was interpreted as the main contributor for the transport of the hydrogen bubbles away from the cathode and towards the cavity wall and therefore at the origin of the macrostructures as seen in Figure 2.

On the HC geometry (Fig. 7), the reduction of the bath flow from 20 lpm to 10 lpm had a smaller impact on the z peak bath velocity, as it only went to half its original value at 20 lpm. Also, for the HC, the vortices are characterised by a smaller dimension, if projected to the cavity length; and less intense, smaller bath velocities both on the z and r directions.

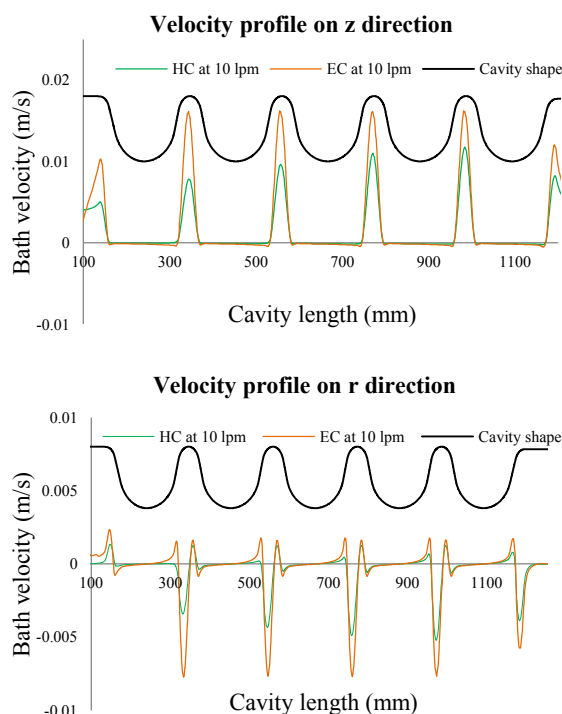


Figure 8: Bath velocity components profile comparison between the EC and HC geometries at 10 lpm.

In Figure 8 are direct comparisons between the EC and the HC geometries at the most interesting bath flow, 10 lpm. For both cathode geometries, it's possible to observe that the bath velocity in the z direction is very low near the equator and it increases sharply near the iris; however, this velocity gap is smaller for the HC than for the EC. In the radial direction bath speed representation, it's possible to identify several vortices features, but with a less extent and intensity for the HC if compared with the EC. For both velocities representations it's possible to see that the HC gets closer to the EC velocities profiles as it goes from the bottom bath inlet (left) to the cavity top outlet (right).

### ELECTROCHEMICAL BEHAVIOUR

The work presented above, has put into evidence the advantage of new HC over the previous EC geometry in terms of bath velocity distribution, but is of utmost importance that it has also a good electrochemical behaviour.

### Minimum Working Potential

The data shown hereafter provides already a current density distribution profile, but it only takes into account electrochemical parameters; however, the minimum working voltage is roughly the same independently of the bath speed and/or temperature variations. The difference between the two geometries, in terms of minimum working potential is small and this is consequence of the large anodic plateau as previously mentioned.

In Figure 9 are represented the current density distribution through the cavity arc length as a function of the applied voltage for both the EC and the HC geometries. Each line represents a current density distribution in  $A.m^{-2}$  for its corresponding applied voltage; the shown applied voltage vary from 5 to 13 volts as defined in the upper right legend. On these simulation data, the working conditions were set so that the electropolishing is achieved above  $87 A.m^{-2}$ ; it can be read from Figure 9 that for the EC cathode, the minimum working potential is 8 V, while the HC cathode needs 7 V.

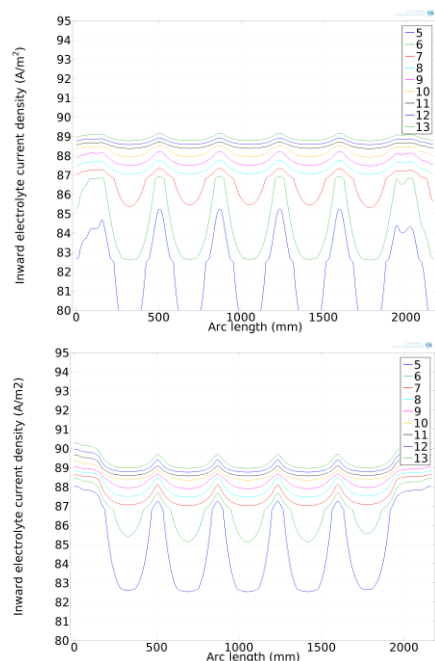


Figure 9: Minimum working voltage evaluation for EC (top) and HC (bottom).

The EC cathode has a better ratio between the maximum and minimum current density if compared with the HC, but the difference becomes irrelevant when the impact of the bath velocity is taken into account on the current density distribution, as shown hereafter.

### Current Density Distribution

Using the methodology described in [4], the impact of the bath flow on the current density distribution, both for EC and HC geometries, was estimated.

The results collected from this method are presented in Figure 10 and reflect to a certain extent the behaviour seen on the fluid dynamic simulations data. Faraday's

laws of electrolysis was used to convert the estimated current density into polishing rate values, see equation 1 hereafter:

$$v_{EP} = k \times \frac{j \times M}{z \times \rho \times C} \quad (1)$$

where  $v_{EP}$  is the polishing rate in  $\mu m/h$ ,  $k$  units conversion constant,  $j$  is the current density in  $A/cm^2$ ,  $M$  is the molar mass of niobium in  $g/mol$ ,  $z$  is the valence number of niobium,  $\rho$  is the volumetric mass of niobium in  $g/cm^3$  and  $C$  is the Faraday constant in  $A.s/mol$ . The values of polishing rate in Figure 10 corresponds to a bath flow of 10 lpm at 10 °C on the SPL fourth cell, both for the EC and HC geometries. The improvement in the uniformity of the polishing rate distribution from EC to HC geometry is quite important near the iris, reducing of roughly to half the polishing rate peak at this location; elsewhere, the polishing rate is quite similar between the two geometries, but still with an advantage towards HC in terms of homogeneity.

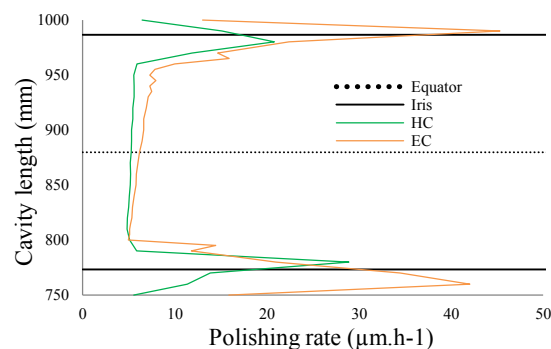


Figure 10: Polishing rate distribution estimation at an average temperature of 10 °C and a bath flow of 10 lpm.

## DATA FROM SPL #2 ELECTROPOLISHING

The data provided by simulation gave enough confidence to produce the new cathode for the HC geometry and to process SPL #2 cavity with it. In order to evaluate the surface finishing evolution, the EP process was stopped after every  $\sim 25 \mu m$ . The first evidence from the operation with this new geometry was the fast clogging of the cathode, the 70  $\mu m$  mesh FEP membrane, but also the 4 mm diameter holes on the copper structure. The cathode could not be recovered completely by cleaning and the accumulation of material from run to run increased.

In total, the SPL #2 cavity had nine runs; the first two runs went smoothly with a constant total current around 130 A ( $76 A.m^{-2}$  at 8V), but the following runs saw a decreasing of this value down to 90 A ( $52 A.m^{-2}$  at 8V) as well as an increasing instability on the total current records and this even after replacing the bath by a new one; the average working temperature was 9.9 °C and the bath flow 9 lpm. The achieved surface finishing improved until the 6<sup>th</sup> run (see Figure 11). The main macrostructures

still visible were the ones already present before the EP, such as the mechanically polished areas, the deformation lines or tool marks; the absence of grooves and pinholes is quite evident namely on the mechanically polished areas.



Figure 11: SPL #2 inner surface after 120  $\mu\text{m}$  EP. Left is the equator and right the iris with a noticeable mechanically polished area.

The 7<sup>th</sup> and 8<sup>th</sup> run were performed without an intermediate stop, and the outcome was the fall of clogging products, from the cathode and membrane, onto the cavity wall. This incident had a negative impact on the surface finishing, with the formation of stains with a rougher surface (see Figure 12) and the surface appearance became slightly less shiny; this incident affected mainly the lower half cells.



Figure 12: SPL #2 representative lower half cell after the 7<sup>th</sup> and 8<sup>th</sup> runs (170  $\mu\text{m}$  EP).

## CONCLUSIONS

The three main modifications introduced on the vertical EP of SPL #2 cavity had a positive impact on the surface finishing. The use of a hollow cathode together with the reduction of the flow rate contributed to an even bath velocity distribution and consequently a more homogeneous, although smaller, EP rate; the introduction of a membrane together with the two other previous modifications, allowed the elimination or at least a significant reduction of grooves and pinholes.

On the other hand, the decrease of the bath flow and consequently bath velocity, increased the bath diffusion layer thickness which decreases the EP efficiency to eliminate macrostructures; also, the clogging of the cathode holes and membrane had a negative impact on the EP velocity and on the surface finishing, namely after two consecutive runs and where the accumulation of copper hydroxides became too important and ended by falling into the cavity surface. An alternative material for the

cathode is already in study and this within the ones commonly used for this application.

The surface finishing achieved on SPL #2, on the CERN vertical EP installation, with the new cathode geometry and new operation parameters was only limited by the initial poor surface condition. There was no evidence of formation of defects related to the EP process like pinholes or grooves. Related radio frequency measurements showed a consequent improvement from SPL #1 to SPL #2 [7].

## REFERENCES

- [1] H. Diepers, O. Schmidt, H. Martens and F.S. Sun, "A New Method of Electropolishing Niobium", Phys. Letters, volume 37A, number 2 (1971) 139.
- [2] S. Calatroni et al., "Status of EP simulations and facilities for the SPL", LINAC10, Tsukuba, Japan (2010).
- [3] L. M. A. Ferreira et al., "Niobium cavity electropolishing modelling and optimisation", SRF2013, Paris, France (2013).
- [4] L. M. A. Ferreira et al., "Electropolishing simulation on full scale radio frequency elliptical structures", LINAC14, Geneva, Switzerland (2014).
- [5] F. Eozenou et al., "Development of an advanced electropolishing setup for multicell high gradient niobium cavities", Phys. Rev. STAccel. Beams 15, 083501 (2012).
- [6] F. Eozenou et al., "Development of vertical electropolishing process applied on 1300 and 704 MHz superconducting niobium resonators", Phys. Rev. ST Accel. Beams 17, 083501 (2014).
- [7] A. Macpherson, "CERN's Bulk Niobium High Gradient SRF Programme: Developments and Recent Cold Test Results", MOPB074, SRF2015, Whistler, Canada (2015).